



This is a repository copy of *Plasma polymerization of isopentyl nitrite at atmospheric pressure: gas phase analysis and surface chemistry*.

White Rose Research Online URL for this paper:

<https://eprints.whiterose.ac.uk/208705/>

Version: Published Version

---

**Article:**

Wang, Y. orcid.org/0009-0006-4353-9278, Robson, A.J. orcid.org/0000-0002-1449-9477, Simon, S. et al. (2 more authors) (2024) Plasma polymerization of isopentyl nitrite at atmospheric pressure: gas phase analysis and surface chemistry. *Plasma Processes and Polymers*, 21 (5). e2300162. ISSN 1612-8850

<https://doi.org/10.1002/ppap.202300162>

---

**Reuse**

This article is distributed under the terms of the Creative Commons Attribution-NonCommercial (CC BY-NC) licence. This licence allows you to remix, tweak, and build upon this work non-commercially, and any new works must also acknowledge the authors and be non-commercial. You don't have to license any derivative works on the same terms. More information and the full terms of the licence here: <https://creativecommons.org/licenses/>

**Takedown**

If you consider content in White Rose Research Online to be in breach of UK law, please notify us by emailing [eprints@whiterose.ac.uk](mailto:eprints@whiterose.ac.uk) including the URL of the record and the reason for the withdrawal request.





[eprints@whiterose.ac.uk](mailto:eprints@whiterose.ac.uk)  
<https://eprints.whiterose.ac.uk/>

## RESEARCH ARTICLE

PLASMA PROCESSES  
AND POLYMERS

# Plasma polymerization of isopentyl nitrite at atmospheric pressure: Gas phase analysis and surface chemistry

Yong Wang<sup>1</sup>  | Alexander J. Robson<sup>2</sup> | Stephane Simon<sup>1</sup> | Robert D. Short<sup>2</sup> | James W. Bradley<sup>1</sup> 

<sup>1</sup>Department of Electrical Engineering and Electronics, Technological Plasmas Group, University of Liverpool, Liverpool, UK

<sup>2</sup>Department of Chemistry, University of Sheffield, Sheffield, UK

## Correspondence

James W. Bradley, Department of Electrical Engineering and Electronics, University of Liverpool, Liverpool, L69 3GJ, UK.

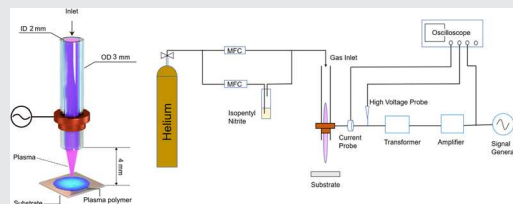
Email: [jbradley@liverpool.ac.uk](mailto:jbradley@liverpool.ac.uk)

## Funding information

Chinese Scholarship Council; Engineering and Physical Sciences Research Council, Grant/Award Numbers: EP/S005153/1, EP/S004505/1

## Abstract

Nitric oxide (NO)-releasing coatings have promising potential for biomedical applications notably in implant safety and wound dressing by promoting healing and reducing bacterial growth. Yet, the production of NO-films remains difficult through classic approaches. In this study, plasma polymerized NO-coatings are produced using a helium-isopentyl nitrite mixture under two power settings and deposited on aluminum samples. Analyses of the plasma phase by mass spectroscopy reveal the presence of nitrosoxy groups (O–N=O) in monomer and quasi-monomer at low power, and a higher fragmentation rate at high power. Static and no-static samples are made and analyzed by X-ray photoelectron spectroscopy showing the presence of these group for both power conditions, with a better retention on the sample's center for the latest.



## KEYWORDS

atmospheric-pressure plasma jet, film characterization, mass spectrometry, plasma polymerization, XPS

## 1 | INTRODUCTION

Bacterial contamination of medical devices and implants remain a significant global health issue. Biofilms, which are assemblages of bacteria adhering on surfaces, are inherently more resistant to antibiotics and have been identified as a leading cause of these concerns.<sup>[1]</sup> Despite rigorous best practices and safety controls, the United States alone has reported over 750 000 implant-related infections (IRIs) annually.<sup>[2]</sup> Such infections not

only lead to severe complications, including the necessity for revision surgeries and prolonged recoveries, but also escalate the consumption of antibiotics. Thus, favoring bacterial resistance to common treatments.<sup>[3]</sup> Over the past decade, antibiotics that were once potent against individual, free-floating (planktonic) bacteria have become less effective against these biofilms.<sup>[4]</sup> As a result of these IRIs, more than 25 000 patients succumb every year in the United States alone.<sup>[5]</sup>

This is an open access article under the terms of the [Creative Commons Attribution-NonCommercial](https://creativecommons.org/licenses/by-nc/4.0/) License, which permits use, distribution and reproduction in any medium, provided the original work is properly cited and is not used for commercial purposes.

© 2024 The Authors. *Plasma Processes and Polymers* published by Wiley-VCH GmbH.

New strategies are in development using nitric oxide (NO) molecules as potential treatment. NO plays an important role in a wide variety of biological systems such as combating infection by exerting antimicrobial effects on pathogens, inducing apoptosis through DNA/proteins damage, preventing thrombosis by inhibiting platelet aggregation, and vasodilation to maintain proper blood flow.<sup>[6,7]</sup> In addition, the effects of NO are often localized due to its short half-life, high diffusion, and reactivity.<sup>[8]</sup> Yet, production of NO delivery media remains complex, mostly due to the short lifespan of most NO donors and the cost of classic chemical production techniques.<sup>[9]</sup>

Plasma polymerization has been actively investigated over many years notably in low-pressure plasma technologies, where volatile organic compounds defined as monomers are used to produce polymer thin films.<sup>[10]</sup> Such films were found to promote the substrate's electrical, optical, or mechanical properties with several applications in industries (i.e., electronics, optoelectronics, aerospace, packaging, chemical surface properties, etc.).<sup>[11–14]</sup> Vacuum-based devices are commonly used in polymerization processes; yet, research groups reported development of new techniques using atmospheric pressure plasmas.<sup>[15,16]</sup> Recent advances in this field have shown promising results and better understanding on the chemical pathways and design optimization.<sup>[17,18]</sup>

In this study, an atmospheric-pressure plasma jet (APPJ) was used for the polymerization of isopentyl nitrite (IPN). This precursor is known for its ability to produce coatings rich in NO functional groups,<sup>[19]</sup> and releasing NO molecules upon contact with biological fluids such as blood or interstitial fluid.<sup>[20]</sup> To investigate the impact of the plasma discharge on the polymerization process, two power settings were selected and the resulting gas phase chemistry was analyzed using mass spectrometry. Both positive and negative ions scans were done at different nozzle-orifice distance to provide a better understanding on the reactions occurring during plasma polymerization. Finally, to highlight the quality of the NO-films formed, samples were coated in a static and nonstatic fashion at either 4- or 6-mm nozzle-sample gap and analyzed by X-ray photoelectron spectroscopy (XPS). These results demonstrate that the initial plasma parameters have a clear impact on the quality of the polymerization by either favoring or not fragmentation, but also indicate that nozzle-sample distance and motion had a significant impact on the film retention quality.

## 2 | EXPERIMENTAL SECTION

### 2.1 | Experimental setup

The plasma jet consists of a cylindrical dielectric barrier discharge (DBD) where the dielectric was a quartz tube of 10 cm in length with an inner and outer diameter of, respectively, 2 and 3 mm. The powered electrode consisted of a copper ring placed 10 mm from the quartz tube extremity and connected to a custom-made power supply. The power supply consisted of a signal generator (TG 2000), a power amplifier (STA- 800), and a home-made transformer built at the University of Liverpool. In this work, a fixed voltage of 9 kV peak-to-peak was selected at two frequencies 5 and 20 kHz defined as, respectively, low- and high-power modes.

Helium (BOC, UN 1046) was used as a gas carrier and the main line was divided to allow the introduction of IPN (97%, CAS 110-46-3, Fisher Scientific, used without further purification) vapors into the system. The flow rate of the main channel was set at two standard liters per minute, where the mixture helium-IPN was set at 20 cubic centimeters per minute. A schematic of the DBD and plasma setup is reported in Figure 1.

The signals of the applied voltage and current were recorded using a digital oscilloscope (DPO 4034B; Tektronix) and measured using respectively a Pintek high-voltage probe (HVP-15HF), and a Pearson current probe (model 2877; Pearson). The plasma discharge power was monitored in real-time by multiplying voltage and current signals on the oscilloscope, giving the instantaneous power which was averaged over multiple cycles to obtain the mean power.

For the low-power mode, an average power of 0.8 W was measured at a frequency of 5 kHz, whereas an average power of 5.1 W was measured at 20 kHz. The temperature of the substrate before and after 20 min static deposition was measured using a thermocouple (Type K; RS Pro), connected to a thermometer (72-7712; TENMA) for both power mode.

Before plasma polymerization, aluminum substrates (1 × 1 cm, Purity 99.5%; Advent Research Materials Ltd.) were placed into a beaker containing isopropanol and cleaned in an ultrasonic bath for 3 min. For the deposition, the samples were either placed static under the jet nozzle or moved linearly (*x*-*y* direction) using a movable stage. In the first scenario, the nozzle-sample gap distance was set at either 4 or 6 mm and treated for a total period of 20 min at either low or high power. When placed on the movable stage, the gap distance was set at 6 mm and the stage moved the sample every 1 mm in the

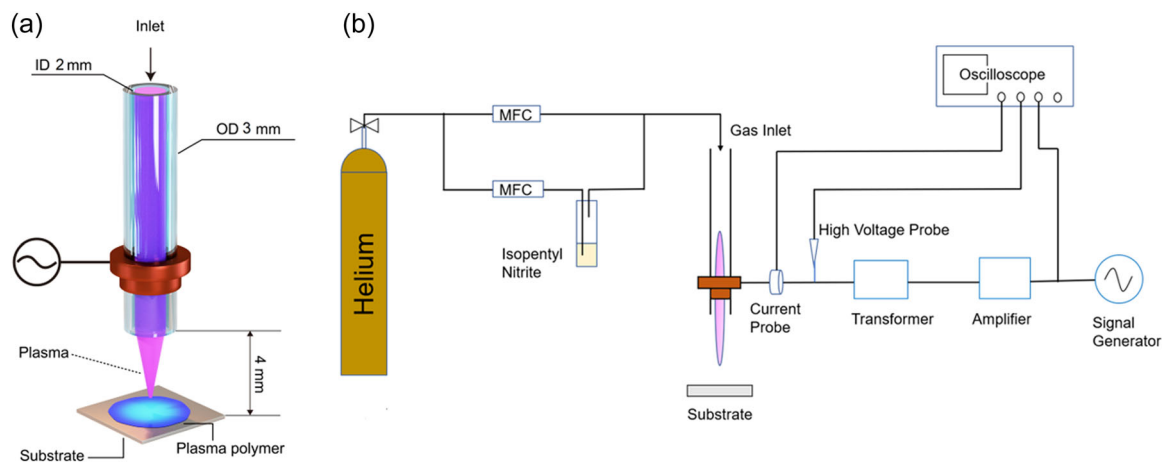


**FIGURE 1** Schematic of (a) the plasma jet over a substrate and (b) the experimental setup for the plasma deposition of nitric oxide. MFC, mass flow controller.

selected direction with a retention time of 30 s at each step and the jet operated only at low power mode.

A quadrupole mass spectrometer (model HPR-60; Hiden Analytical) was used to measure both positive and negative ions formed in the plasma. A sample orifice of 100  $\mu\text{m}$  was selected and the plasma plume was aligned with the orifice center, the nozzle-orifice distance was varied from 2 to 10 mm.

After exposing the aluminum substrate to the plasma polymerized IPN, the samples were analyzed by XPS (Kratos Analytical AXIS Supra) at the University of Lancaster. The analysis used a monochromatic source Al K $\alpha$  1486.7 eV, operating at 15 kV, 15 mA, and equipped with an electron flood gun for charge neutralization. Binding energies were calculated with reference to the C1s peak at 285 eV.

### 3 | RESULTS AND DISCUSSION

#### 3.1 | Gas phase analysis

The gas phase chemistry plays a crucial role in plasma polymerization as already reported by various groups.<sup>[21,22]</sup> For example, the ion chemistry of a pure He jet into the air consists mainly of the generation of water clusters, nitrogen and oxygen ions. When introducing IPN, the ion chemistry will be drastically modified owing to the formation of various new species such as cations, anions, excited molecules and radicals.<sup>[23]</sup> Such mechanisms are difficult to explain due to the fast and high reactivity of the processes occurring within the plasma.<sup>[24]</sup> In this section, we report our main observations obtained for two plasma conditions set at

either low or high power with a nozzle-orifice distance of 6 mm.

##### 3.1.1 | Analysis of the positive ions

Figure 2 presents the mass spectra of positive ions, respectively, at low and high power. For both powers, the spectra revealed similar positive ions usually found in a pure He plasma in air such as helium ( $m/z=4$ ), water cluster ( $m/z=18$ ), nitrogen ( $m/z=14$  and 28), and oxygen ( $m/z=16$  and 32).<sup>[25]</sup> Additionally, the monomer ions  $[M]^+$  ( $m/z=117$ ) and its quasi-monomers  $[M-H]^+$  ( $m/z=116$ ) and  $[M+H]^+$  ( $m/z=118$ ) were also detected. The generation of the dimer is restricted by the operational mode of the plasma jet, with only the high-power mode able to produce  $[2M+H]^+$  ( $m/z=235$ ). The main difference lies in the level of fragmentation of the monomer with the high-power mode being more efficient. For both conditions, the main fragments were detected at  $m/z=43$  ( $C_3H_7^+$ ),  $m/z=57$  ( $C_4H_9^+$ ),  $m/z=71$  ( $C_5H_{11}^+$ ), and  $m/z=87$  ( $C_5H_{11}O^+$ ), representing the dissociation of different bonds from the monomer shown in Figure 2c.

Furthermore, it is classic to observe heavy ions formed by recombination between fragments and  $[M]^+$ . These ions were detected at  $m/z=160$ ,  $m/z=174$ ,  $m/z=188$ , and  $m/z=204$  corresponding to the recombination between  $[M]^+$  ( $m/z=117$ ) and, respectively,  $C_3H_7^+$ ,  $C_4H_9^+$ ,  $C_5H_{11}^+$ , and  $C_5H_{11}O^+$ . As observed, the majority of the fragments are based on long carbon chains, suggesting that within the plasma plume's positive ions, nitrosoxy groups are confined predominantly to the monomer and quasi-monomer ions.

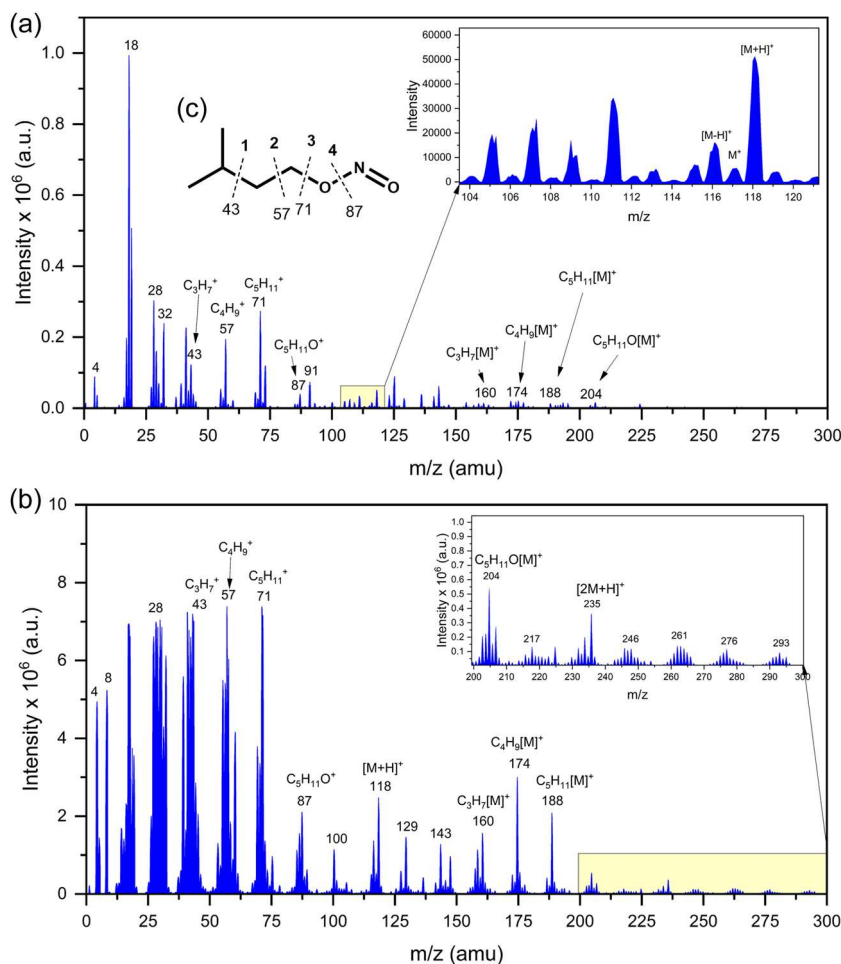


**FIGURE 2** Mass spectra of the positive ions in a He-isopentyl nitrite (IPN) plasma obtained at (a) low power and (b) high power for a nozzle-orifice gap of 6 mm, IPN formula with the different bonds in (c).

Figure 3 reports the peak intensity of  $[M]^+$ ,  $[M-H]^+$ , and  $[M+H]^+$  measured for different nozzle-orifice distances. For both power conditions, the intensity of the monomer and quasi-monomers decreased with the nozzle-orifice distance with the high power showing a sharper variation than the low power. Compared to the low power mode, the changing trend of those three ions is more consistent at high power mode. This is because the jet is operated at a stable condition at a relatively higher input power.<sup>[26]</sup> However, at low input power, there is not enough power to sustain a stable discharge, resulting in a more stochastic and chaotic discharge in the plasma plume. Finally, the production of quasi-monomers was found to be higher than the monomer for both power modes.

### 3.1.2 | Analysis of the negative ions

Figure 4 reports the spectra obtained for the negative ions for both low (Figure 4a) and high power (Figure 4b). Negative

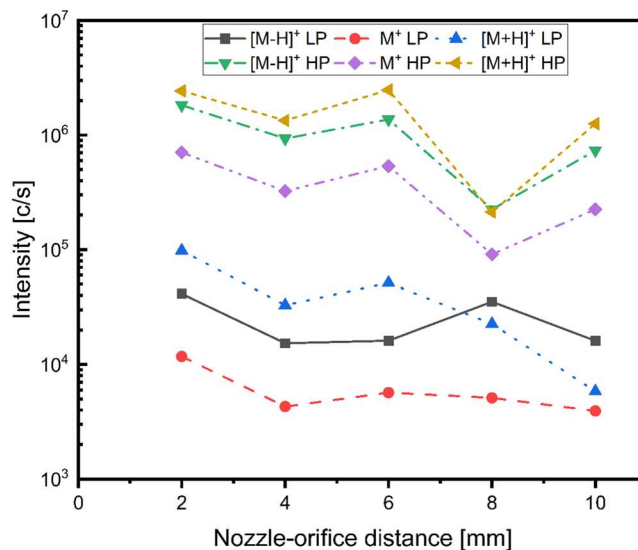
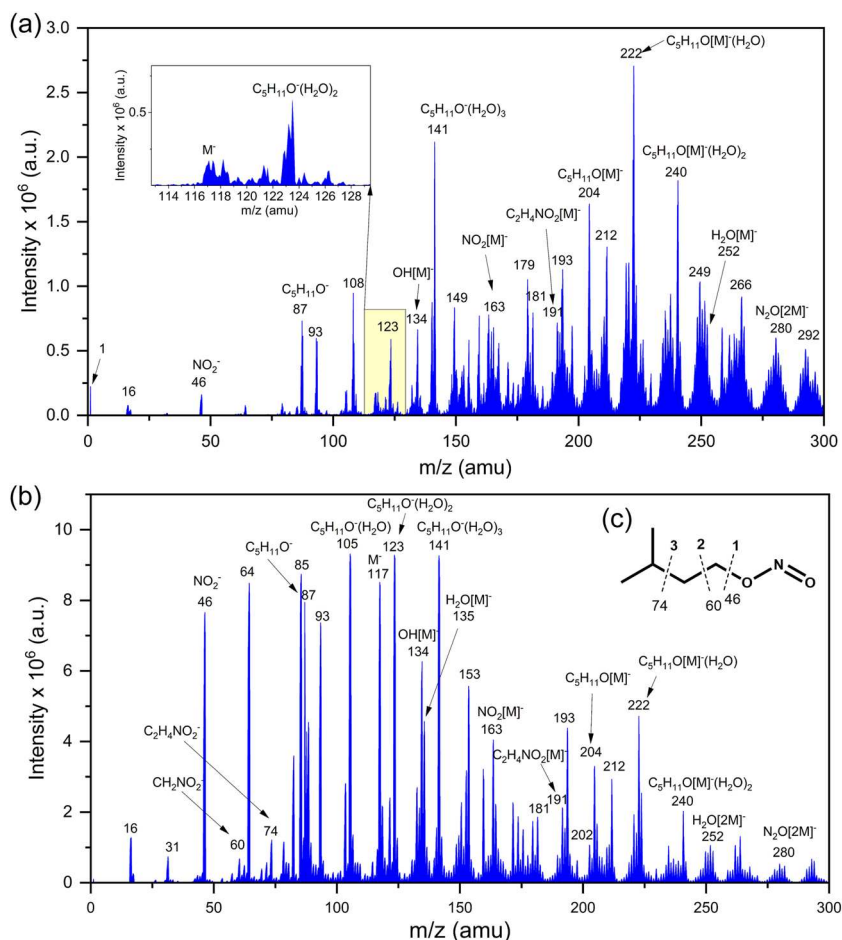


**FIGURE 3** Evolution of  $[M-H]^+$ ,  $[M]^+$ , and  $[M+H]^+$  at different nozzle-orifice distances for both low- and high-power mode.



**FIGURE 4** Mass spectra of the negative ions of the He-isopentyl nitrite (IPN) mixture obtained at (a) low- and (b) high-power mode. IPN formula with the different bonds in (c).



ions are mainly produced through direct electron attachment, dissociative electron attachment and three-body electron attachment.<sup>[27]</sup> Electrons with low energy will combine directly with the monomer to form  $[M]^-$  at  $m/z = 117$ , whereas dissociative electron attachment will result in the formation of several fragments such as  $m/z = 87$  ( $C_5H_{11}O^-$ ).<sup>[28]</sup> Other fragments were also found at  $m/z = 46$ , 60, and 74 amu, corresponding to the bond break in Figure 4c. These fragments appear to contain nitrosoxy groups except for  $NO^-$  ( $m/z = 30$ ). As observed with the positive ions, the fragments produced during the process will recombine with the monomer to form heavier elements such as  $m/z = 163$  ( $NO_2[M]^-$ ),  $m/z = 191$  ( $C_2H_4NO_2[M]^-$ ), and  $m/z = 204$  ( $C_5H_{11}NO[M]^-$ ). As seen in other works using heptylamine and acrylic acid as monomer, the spectra displayed similar recombination events involving monomers or fragments with other minor molecules.<sup>[16,29]</sup> For instance,  $m/z = 134$  suggests a recombination between  $OH^-$  and the IPN monomer, whereas  $m/z = 105$ , 123, and 141 are recombination of  $C_5H_{11}O^-$  with various water molecules.

Clearly, in low-power mode, the formation of heavier negative oligomers is favored, whereas in high-power mode the intensity of fragments is significantly amplified. Regarding other negative oligomers that are not

formed through recombination of fragments with monomers, more intricate reactions such as rearrangement could be taking place. Involving concurrent breaking and forming of chemical bonds, often accompanied by the release of neutral fragment molecules.<sup>[30,31]</sup>

In summary, the ionic species present in a helium-IPN plasma are dominantly under the form of fragments and oligomers, arising from the recombination between fragments, monomers, and water molecules. For the positive ions, the IPN monomers undergo greater fragmentation at high power, resulting in a mass spectrum with more intense heavier ion signals compared to low power. Conversely, for the negative ions, at high power the fragment intensity substantially increases, whereas the low power favors the formation of heavier negative oligomers.

### 3.2 | Characterization of the NO thin films

To study the surface chemical distribution of the IPN films, XPS analyses were done over five different points distributed linearly and spaced every 2 mm across each

**TABLE 1** XPS distribution of atomic percentage at different experimental conditions.

| Power | Distance (mm) | Elements | Percentage |       |        |      |      |
|-------|---------------|----------|------------|-------|--------|------|------|
|       |               |          | −4 mm      | −2 mm | Center | 2 mm | 4 mm |
| Low   | 4             | C 1s     | 58.5       | 65.7  | 72.1   | 65.6 | 58.6 |
|       |               | N 1s     | 6.2        | 7.8   | 9.9    | 7.4  | 5.9  |
|       |               | O 1s     | 29.9       | 26.1  | 18.2   | 26.6 | 29.9 |
|       |               | Al 2p    | 5.7        | 0.7   | 0      | 0.5  | 5.9  |
| Low   | 6             | C 1s     | 60.0       | 64.9  | 69.5   | 65.0 | 63.1 |
|       |               | N 1s     | 5.0        | 4.9   | 8.8    | 6.3  | 3.3  |
|       |               | O 1s     | 30.1       | 29.2  | 21.7   | 28.0 | 30.0 |
|       |               | Al 2p    | 4.9        | 1     | 0      | 0.8  | 3.6  |
| High  | 4             | C 1s     | 65.0       | 68.8  | 73.2   | 66.3 | 64.5 |
|       |               | N 1s     | 7.0        | 8.1   | 9.4    | 7.1  | 7.3  |
|       |               | O 1s     | 26.6       | 23.2  | 17.4   | 26.0 | 25.8 |
|       |               | Al 2p    | 1.4        | 0     | 0      | 0.7  | 2.5  |
| High  | 6             | C 1s     | 64.7       | 65.9  | 69.2   | 66.8 | 53.8 |
|       |               | N 1s     | 6.2        | 6.6   | 8.8    | 6.6  | 5.9  |
|       |               | O 1s     | 27.8       | 27.2  | 22.0   | 26.3 | 28.2 |
|       |               | Al 2p    | 1.0        | 0.4   | 0      | 0.4  | 2.1  |

Abbreviation: XPS, X-ray photoelectron spectroscopy.

**TABLE 2** Functional groups distribution at different experimental conditions.

| Power | Distance (mm) | Functional groups | Percentage |       |        |      |       |
|-------|---------------|-------------------|------------|-------|--------|------|-------|
|       |               |                   | −4 mm      | −2 mm | Center | 2 mm | 4 mm  |
| Low   | 4             | N–C               | 12.5       | 18.9  | 30.4   | 17.0 | 12.6  |
|       |               | N–O               | 31.8       | 43.7  | 62.1   | 45.6 | 31.2  |
|       |               | N <sup>+</sup>    | 11.0       | 14.8  | 7.0    | 17.8 | 10.4  |
|       |               | O–N=O             | 44.7       | 22.5  | 0.5    | 20.0 | 45.76 |
| Low   | 6             | N–C               | 16.2       | 24.9  | 70.8   | 31.7 | 16.3  |
|       |               | N–O               | 21.1       | 26.0  | 20.6   | 30.4 | 22.5  |
|       |               | N <sup>+</sup>    | 7.7        | 14.4  | 6.7    | 23.4 | 9.6   |
|       |               | O–N=O             | 55.0       | 34.7  | 1.9    | 14.6 | 52.4  |
| High  | 4             | N–C               | 40.1       | 53.7  | 63.1   | 45.2 | 43.2  |
|       |               | N–O               | 21.9       | 26.9  | 28.7   | 25.4 | 18.3  |
|       |               | N <sup>+</sup>    | 8.2        | 12.2  | 8.0    | 14.8 | 8.9   |
|       |               | O–N=O             | 29.7       | 7.3   | 0.2    | 14.5 | 29.6  |
| High  | 6             | N–C               | 12.5       | 18.9  | 30.4   | 16.9 | 12.6  |
|       |               | N–O               | 31.8       | 43.7  | 62.1   | 45.6 | 31.2  |
|       |               | N <sup>+</sup>    | 11.0       | 14.8  | 7.0    | 17.8 | 10.4  |
|       |               | O–N=O             | 44.7       | 22.5  | 0.5    | 19.7 | 45.8  |

sample. Each point was referred to as  $-4$ ,  $-2$ ,  $+2$ , and  $+4$  mm, in regard to the center point (i.e.,  $0$  mm) aligned with the jet nozzle. The substrate's surface temperature was recorded during plasma exposure, showing at low power an increase of  $2.4^{\circ}\text{C}$  at the sample's center and  $2^{\circ}\text{C}$  on the edges after a  $20$  min exposure. At high power, the overall surface temperature increased by  $3.1^{\circ}\text{C}$  after  $20$  min.

Table 1 shows trends in atomic composition across five points on samples polymerized under different conditions. The atomic percentages measured at the center points align closely with the expected values for an adequately dense IPN coating, which theoretically contains  $67.5\%$  carbon,  $12.5\%$  nitrogen, and  $25\%$  oxygen.<sup>[19]</sup> The highest percentage of carbon and nitrogen are consistently found at the center point. There is a general decrease in carbon and nitrogen composition moving away from the center to the edges. The increase of aluminum signal when moving away from the center indicates a thinner film

coverage at the edges. Aluminum oxide may also contribute to relatively increase oxygen content at the edges. Besides, for the same sample-nozzle distance, similar atomic percentage were found at the center point, suggesting that the atomic percentage at the center point is distance-related to the jet nozzle.

In the Electronic Supplementary Information (ESI\*), the high-resolution fitting for the N 1s peak is presented for films deposited at a frequency of  $5$  kHz with a nozzle-sample distance of  $4$  mm, specifically at the  $+4$  mm location. The spectral analysis identified four distinct components: N-C at  $399.3$  eV, N-O at  $400$  eV, N+ at  $401.6$  eV, and O-N=O at  $405.6$  eV. Table 2 presents the distribution of different nitrogen-containing functional groups on films deposited at different experimental conditions. The concentration of N-C tends to be highest at the center point for both power settings and distances and decreasing towards the edges. Similar to N-C, N-O shows a higher concentration at the center, which then diminishes toward the  $-4$  and  $+4$  mm points. The

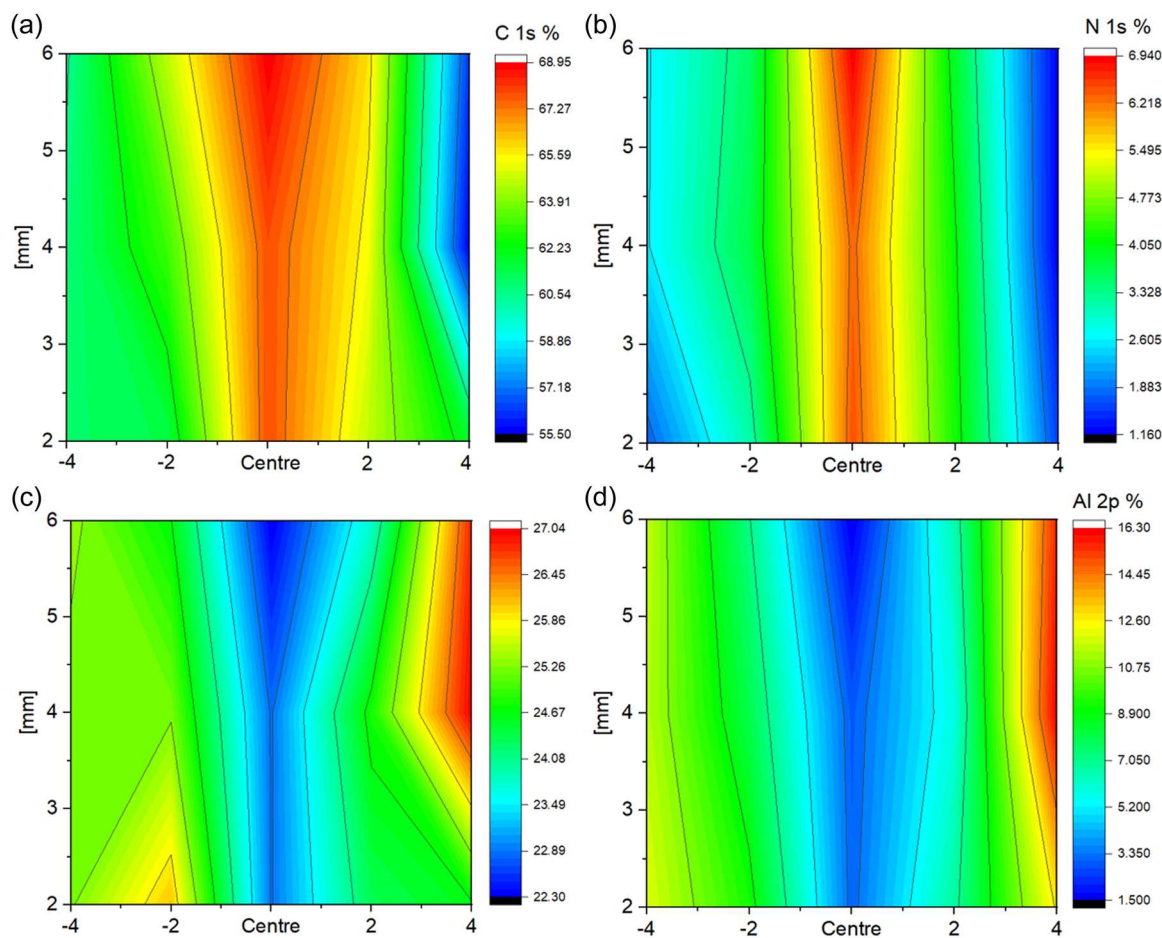


**FIGURE 5** Surface chemical composition distributions of (a) C 1s, (b) N 1s, (c) O 1s, and (d) Al 2p when the deposition trajectory (along the y axis direction) is a line. The deposition step is  $1$  mm with the jet operated at low power mode and a  $30$ -s stay at each position.



presence of  $N^+$  is more evenly distributed, though it generally decreases at the center compared to the  $-2$  and  $+2$  mm points. The desired functional group is more abundant at the edges rather than the center across all conditions, particularly at the  $+4$  mm point. However, despite the lower presence of the targeted  $O-N=O$  functional group at the center, the distribution pattern across the sample suggests a significant retention of this functional group, especially at the edges.

Figure 5 shows the surface chemical composition when the deposition employed the movable stage. For these samples, five-point were taken across each sample along the trajectory. The obtained atomic percentage at the center line corresponds to an average value of 68.2% C, 6.6% N, 22.7% O, and 2.5% Al. As reported previously the different elements percentage present a gradient going from the center to the periphery of the deposition path. The C 1s and N 1s see their highest percentage at the center, while for O 1s and Al 2p, their percentages were found higher

on the substrate edges. Similar to Table 1, the variation in Al percentage indicates a thicker coating on the center compared to the edges of the substrate.

Figure 6 shows the different functional groups on the surface when the deposition was done linearly. The average percentage of N-C and O-N=O at the central line is 67.5% and 3.2%, respectively. The O-N=O content along the central line was found higher compared to the static samples. However, the mean O-N=O content drops to 11.6% at  $\pm 2$  mm and 10.4% at  $\pm 4$  mm falling below the levels observed in static depositions. For N-C and  $N^+$ , a less symmetric distribution was observed. This phenomenon could be explained by the fact that the plasma jet might induce variable heating across the aluminum substrate; leading to temperature gradients affecting the surface species' movement and reaction rates.<sup>[32]</sup> Additionally, uneven diffusion or scattering of reactive species might occur, influenced by electric or magnetic fields on or near the surface.<sup>[26]</sup>

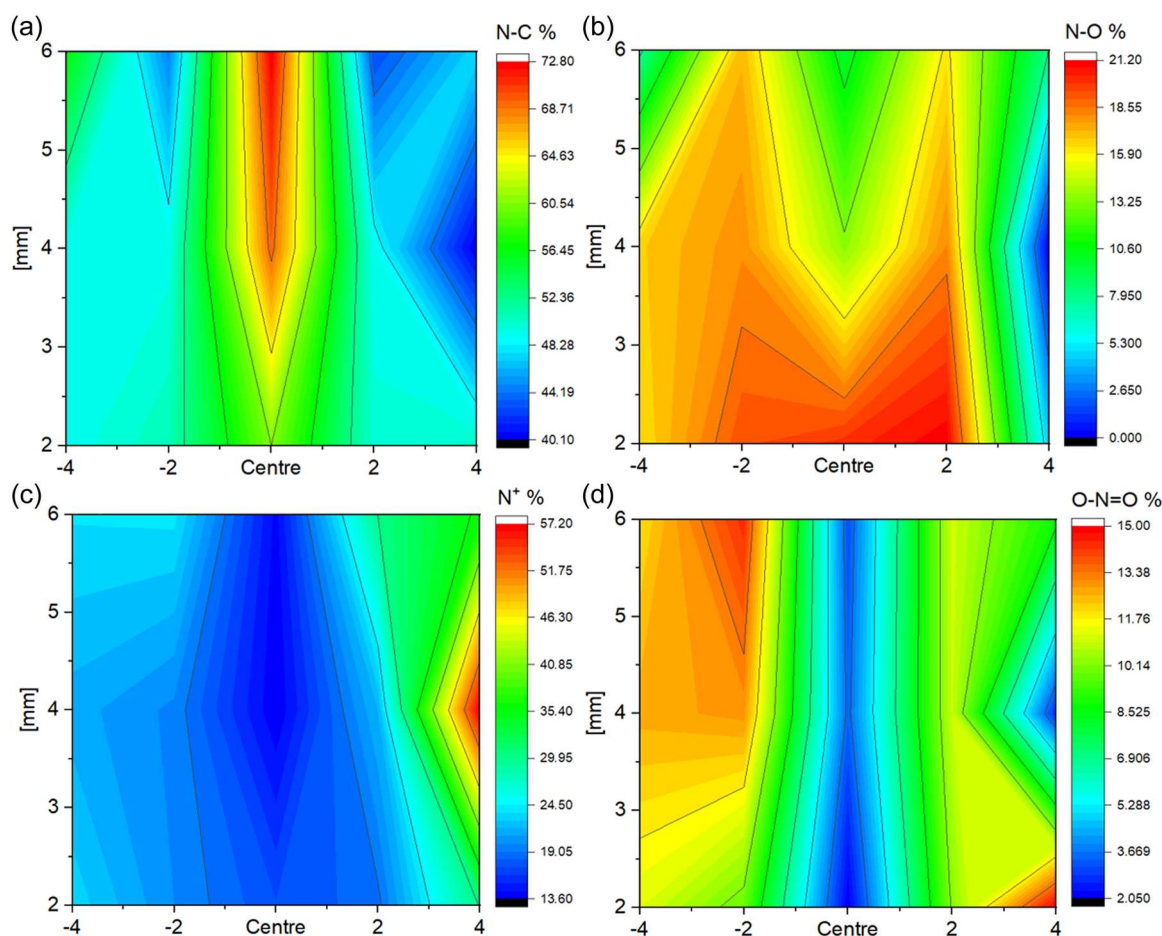


**FIGURE 6** Distribution of the functional groups (a, N-C; b, N-O; c,  $N^+$ ; and d, O-N=O) on the surface when the deposition path (along the y axis direction) is linear.

## 4 | CONCLUSIONS

The integration of O–N=O groups onto aluminum substrates was successfully carried out using an APPJ, utilizing varying power settings and sample movement patterns. Gas phase compositions were examined through mass spectrometry, analyzing both positive and negative ions. The findings reveal that higher power settings led to a greater degree of IPN monomer fragmentation and an abundance of heavier positive ions, whereas lower power settings promote the formation of heavier negative oligomers. While dynamically moving the sample beneath the jet resulted in increasing O–N=O group retention at the center compared to static deposition, the peripheral regions exhibited greater O–N=O retention in static deposition and extended exposure time. A consistent observation is that O–N=O concentrations at the center are lower than the edges. For static depositions, a lower power with a 6 mm nozzle-sample distance proved most effective for enhancing O–N=O retention centrally. These insights indicate that movable deposition techniques are preferable when employing IPN monomers.

## AUTHOR CONTRIBUTIONS

Yong Wang, Stephane Simon, and James W. Bradley contributed to the study conception and design. Gas phase analyses were conducted by Yong Wang. XPS analyses were conducted by Alexander J. Robson, Yong Wang, Stephane Simon, and James W. Bradley wrote the manuscript with input from all authors.

## ACKNOWLEDGMENTS

The authors thank the Engineering and Physical Sciences Research Council (EPSRC) for supporting this work with grants EP/S005153/1 and EP/S004505/1. The authors are also thankful to the Chinese Scholarship Council for their support.

## DATA AVAILABILITY STATEMENT

The data that support the findings of this study are available from the corresponding author upon reasonable request.

## ORCID

Yong Wang  <http://orcid.org/0009-0006-4353-9278>

James W. Bradley  <http://orcid.org/0000-0002-8833-0180>

## REFERENCES

- [1] H. C. Flemming, J. Wingender, U. Szewzyk, P. Steinberg, S. A. Rice, S. Kjelleberg, *Nat. Rev. Microbiol.* **2016**, 14(9), 563.
- [2] P. Chenhao, Z. Zhou, X. Yu, *J. Orthop. Surg. Res.* **2018**, 13.1, 1.
- [3] B. Li, T. J. Webster, *J. Orthop. Res.* **2018**, 36, 22.
- [4] H. Wu, C. Moser, H. Z. Wang, N. Høiby, Z. J. Song, *Int. J. Oral Sci.* **2015**, 7(1), 1.
- [5] J. S. VanEpps, J. G. Younger, *Shock* **2016**, 46(6), 597.
- [6] H. Alimoradi, K. Greish, A. B. Gamble, G. I. Giles, *Pharm. Nanotechnol.* **2019**, 7(4), 279.
- [7] Y. Ying, P. K. Qi, Z. L. Yang, N. Huang, *Biosurface Biotribology* **2015**, 3, 177.
- [8] A. W. Carpenter, M. H. Schoenfisch, *Chem. Soc. Rev.* **2012**, 41(10), 3742.
- [9] T. Yang, A. N. Zelikin, R. Chandrawati, *Adv. Sci.* **2018**, 5(6), 1701043.
- [10] H. Biederman, *Plasma Polymer Films*, World Scientific, London **2004**.
- [11] S. Plog, J. Schneider, M. Walker, A. Schulz, U. Stroth, *Surf. Coat. Technol.* **2011**, 205, S165.
- [12] L. Foroughi Mobarakkeh, R. Jafari, M. Farzaneh, *Adv. Mat. Res.* **2011**, 409, 783.
- [13] X. He, I. Rytöluoto, R. Anyszka, A. Mahtabani, E. Saarimäki, K. Lahti, M. Paajanen, W. Dierkes, A. Blume, *Polymers* **2019**, 11(12), 1957.
- [14] S. Yoshida, K. Hagiwara, T. Hasebe, A. Hotta, *Surf. Coat. Technol.* **2013**, 233, 99.
- [15] S. A. Al-Bataineh, A. A. Cavallaro, A. Michelmore, M. N. Macgregor, J. D. Whittle, K. Vasilev, *Plasma Processes Polym.* **2019**, 16(10), 1900104.
- [16] F. Moix, K. McKay, J. L. Walsh, J. W. Bradley, *Plasma Processes Polym.* **2016**, 13(2), 236.
- [17] L. M. Watkins, A. F. Lee, J. Moir, K. Wilson, *ACS Biomater. Sci. Eng.* **2017**, 3(1), 88.
- [18] W. X. Chen, J. S. Yu, W. Hu, G. L. Chen, *Appl. Surf. Sci.* **2016**, 387, 957.
- [19] T. D. Michl, B. R. Coad, M. Doran, M. Osiecki, M. H. Kafshgari, N. H. Voelcker, A. Hüsler, K. Vasilev, H. J. Griesser, *Chem. Commun.* **2015**, 51(32), 7058.
- [20] N. Fogh-Andersen, B. M. Altura, B. T. Altura, O. Siggaard-Andersen, *Clin. Chem.* **1995**, 41(10), 1522.
- [21] H. K. Yasuda, *Plasma Polymerization*, Academic Press, London **2012**.
- [22] D. Thiry, S. Konstantinidis, J. Cornil, R. Snyders, *Thin Solid Films* **2016**, 606, 19.
- [23] T. Yang, Z. Du, H. Qiu, P. Gao, X. Zhao, H. Wang, Q. Tu, K. Xiong, N. Huang, Z. Yang, *Bioact. Mater.* **2020**, 5(1), 17.
- [24] M. N. Macgregor, A. Michelmore, H. Safizadeh Shirazi, J. Whittle, K. Vasilev, *Chem. Mater.* **2017**, 29(19), 8047.
- [25] J. S. Oh, Y. Aranda-Gonzalvo, J. W. Bradley, *J. Phys. D: Appl. Phys.* **2011**, 44(36), 365202.
- [26] J. L. Walsh, F. Iza, N. B. Janson, V. J. Law, M. G. Kong, *J. Phys. D: Appl. Phys.* **2010**, 43(7), 075201.
- [27] A. Fridman, *Plasma Chemistry*, Cambridge University Press, New York **2008**.
- [28] D. Hegemann, E. Bülbül, B. Hanselmann, U. Schütz, M. Amberg, S. Gaiser, *Plasma Processes Polym.* **2021**, 18(2), 2000176.
- [29] J. S. Oh, J. W. Bradley, *Plasma Processes Polym.* **2013**, 10(10), 839.
- [30] F. Cuyckens, M. Claeys, *J. Mass Spectrom.* **2004**, 39(1), 1.
- [31] N. M. M. Nibbering, *J. Am. Soc. Mass Spectrom.* **2004**, 15(7), 956.

- [32] S. A. Norberg, E. Johnsen, M. J. Kushner, *J. Appl. Phys.* **2015**, *118*(1), 013301.

## SUPPORTING INFORMATION

Additional supporting information can be found online in the Supporting Information section at the end of this article.

**How to cite this article:** Y. Wang, A. J. Robson, S. Simon, R. D. Short, J. W. Bradley, *Plasma. Process. Polym.* **2024**, e2300162.

<https://doi.org/10.1002/ppap.202300162>